Mineralogical Magazine, August 2005, Vol. 69(4), pp. 403–423

The chemistry of allanite from the Daibosatsu Pass, Yamanashi, Japan

M. HOSHINO[1,*], M. KIMATA[1], N. NISHIDA[2], A. KYONO[1], M. SHIMIZU[1] AND S. TAKIZAWA[1]

[1] Doctoral Program in Earth Evolution Sciences, Graduate School of Life and Environmental Sciences, The University of Tsukuba, Ibaraki, 305-8572, Japan
[2] Chemical Analysis Division, Research Facility Centre for Science and Technology, The University of Tsukuba, Ibaraki, 305-8577, Japan

ABSTRACT

The crystal structure of allanite from granitic pegmatite, the Daibosatsu Pass, Yamanashi, Japan, has been refined under the constraint of chemical composition determined by electron microprobe analysis of rare earth elements. Back-scattered-electron images and X-ray element maps of the allanites show that each of their crystal grains has chemically homogeneous distribution of major elements. A typical formula for the chemistry is: $(Ca_{0.920}\square_{0.080})_{\Sigma 1.000}(La_{0.238}Ce_{0.443}Pr_{0.048}Nd_{0.100}Sm_{0.019}Th_{0.042}Mn_{0.008}\square_{0.102})_{\Sigma 1.000}(Al_{0.607}Fe^{3+}_{0.317}Ti_{0.076})_{\Sigma 1.000}(Al_{1.000})(Fe^{2+}_{0.543}Fe^{3+}_{0.365}Mn_{0.055}Mg_{0.037})_{\Sigma 1.000}(SiO_4)(Si_2O_7)O(OH)$.

The crystal structure of allanite, monoclinic, *a* 8.905 (1), *b* 5.7606 (5), *c* 10.123 (1) Å, β 114.78º(1), space group $P2_1/m$, $Z = 2$, has been refined to an unweighted *R* factor of 3.46% for 1459 observed reflections. Although the H atom position was not determined on the Difference-Fourier map, inspection of the bond valence sums demonstrates that the H atom is uniquely located at the O10 atom and involved in a hydrogen bond to O4. A systematic examination as to crystal chemistry of allanites suggests that the isolated SiO_4 tetrahedron has the largest distortion of three kinds of the tetrahedron containing Si_2O_7 groups in the allanite structure. This observation is common to the epidote group minerals, while the larger distortion of *A*2 sites caused by occupancy by *REE* in allanites contrasts with the smaller one of *A* sites in other epidote group minerals. In the allanite groups the bond angles between the O10−H bond and hydrogen bond H···O4 are found to range from 170 to 180º.

Compilation of the chemical compositions of the title allanite and the others from granitic rocks, Japan, which reveals Th-incorporation as the coupled substitution of $3Th^{4+} + \square$ (vacancy) $\rightleftharpoons 4REE^{3+}$, provides an explanation for the observation that higher Th concentrations characterize allanites from the island arcs. The ternary Al_2O_3-Fe_2O_3-Σ*REE* diagram illustrates that allanites are grouped, according to their origins, into three classes suggestive of tectonic backgrounds for the crystallization localities; (1) intracontinental, (2) island arc and (3) continental margin.

KEYWORDS: allanite, Japan, chemistry, tectonic setting, crystal structure, EMPA.

Introduction

ALLANITE, an epidote group mineral [$A_2M_3Si_3O_{12}(OH)$: *A* = Ca, Ce; *M* = Al, Fe], is known as a characteristic accessory mineral in granite, granodiorite, monzonite, syenite, skarns and granite pegmatite (e.g. Deer *et al*., 1986; Gaines *et al*., 1997; Gieré and Sorensen, 2004), and is found in glaucophane schist (Banno, 1993) and garnet lherzolite as well (Yang and Enami, 2003). There are also allanite phenocrysts in acid volcanic rocks (e.g. Mahood and Hildreth, 1983; Chesner and Ettlinger, 1989). The classification of Ercit (2002) permits allanites to be grouped, according to their major *REE* contents, into allanite-(Ce), allanite-(La) and allanite-(Y). Most allanites preferentially incorporate the radioactive elements Th and U, as minor elements (Deer *et al*., 1986), and so allanite often occurs in the

* E-mail: hossy716@arsia.geo.tsukuba.ac.jp
DOI: 10.1180/0026461056940259

metamict state. However a report by Holtstam *et al*. (2003) concluded that non-metamict and unaltered ferriallanite-(Ce) from the Bastäs Fe-Cu-*REE* deposit in Sweden, $CeCaFe^{2+}AlFe^{3+}(SiO_4)(Si_2O_7)O(OH)$, contains neither Th nor U.

Because of the very close spacing of the X-ray lines in the *L* spectra of the *REE*s, accurate electron microprobe analysis (EMPA) of *REE*-bearing minerals is experimentally challenging (Reed and Buckley, 1998; Nishida *et al*., 1999). The modified methods devised through careful measurement of these X-ray lines have improved the quality of the *REE* data collected by EMPA (Reed and Buckley, 1998; Nishida *et al*., 1999), where accelerating voltage of 25 kV is appropriate for quantitative analysis of *REE*. Previously published compositions of allanites from Japan (e.g. Hasegawa, 1957; Nagashima and Nagashima, 1960), except for granitic allanite (Suzuki *et al*., 1990) and metamorphic allanite (Sakai *et al*., 1984; Banno, 1993), were reported before initial use of EMPA. Several authors (Pudovkina and Pyatenko, 1965; Dollase, 1971) have carried out structural determinations of non-metamict allanites since the first refinement of the crystal structure of allanite by Ueda (1955). However, because of the lack of accurate EMPA of *REE* (Reed and Buckley, 1998; Nishida *et al*., 1999), structural refinements of allanites have not been attempted under the fixed constraint of their chemical compositions.

The aims of this study are (1) to determine accurate chemical compositions, resolved by EMPA, of allanites from granitic rocks, Japanese island arc, (2) to define crystal chemistry characteristics of allanites, and (3) to provide

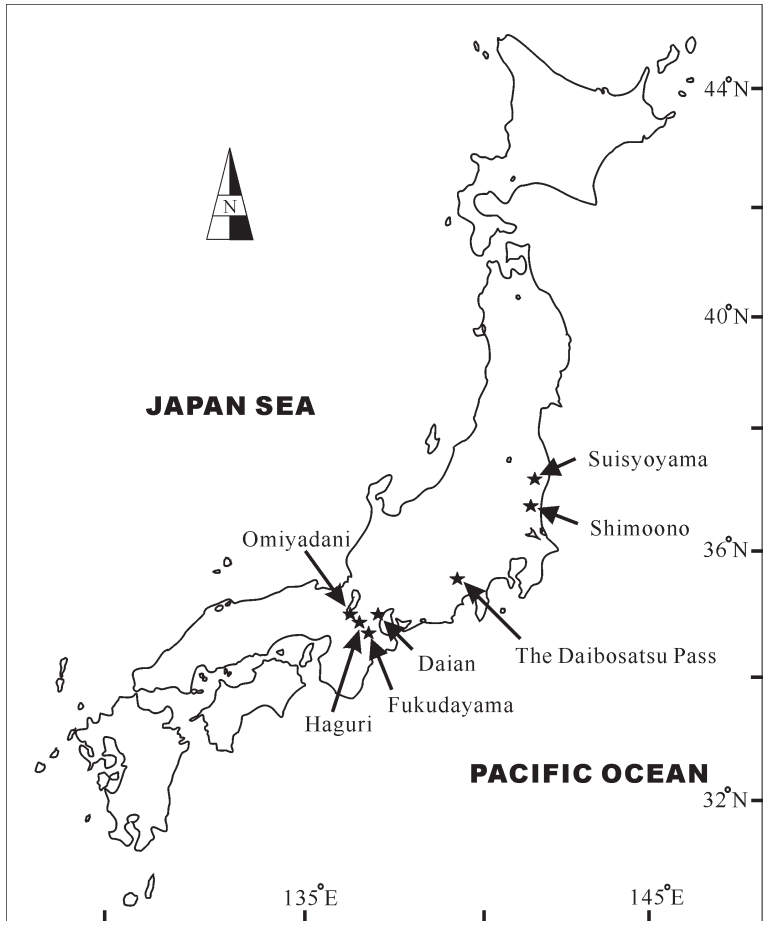

FIG. 1. Occurrences of allanite in Japan.

geochemical backgrounds of tectonics on occurrences of allanites.

Experimental methods

Occurrence and crystal information

The Daibosatsu Pass, in northeast Yamanashi Prefecture, Japan, comprises Tertiary pelitic hornfels (Nagashima and Nagashima, 1960) (Fig. 1). Allanite occurs as a coarse-grained black prismatic crystal in the granitic pegmatite intruding into those rocks together with quartz and a few plagioclases (Fig. 2). Nearby dykes contain scheelite, epidote and ilmenite (Nagashima and Nagashima, 1960). Some allanites completely enclosed by quartz, presumably less permeable to fluid, tend to be in a non-altered and non-metamict state, but this granitic pegmatite is radioactive, as determined by a Geiger-Müller counter.

The allanite crystals range in size from $10 \times 10 \times 25$ mm to $2 \times 2 \times 5$ mm. Figure 3 shows the morphology of allanites from the Daibosatsu Pass and the intracontinental region (Deer *et al*., 1986). The intracontinental morphologies of allanites (with some uncertainty in the mineral identification) show tabular habit (Hintze, 1897; Dana, 1911; Goldschmidt, 1920; Tröger, 1971; Deer *et al*., 1986), whereas allanites from the Daibosatsu Pass are regularly prismatic and euhedral.

Chemical composition

Allanites were analysed for major and minor elements using the EMPA (JXA-8621; JEOL) equipped with three wavelength-dispersive spectrometers. Qualitative analyses were made using 25 kV accelerating potential and 250 nA beam current. The methods for selection of the *REE* peak position recommended by Nishida *et al*. (1999) were applied to the present analysis: the *K* series of X-ray spectra was used for major elements; the *M* series for Th; and the *L* series for *REE*. Measurements of the $L\alpha$ lines for Y, La, Ce and Nd and the $L\beta$ lines for Pr, Sm, Gd and Dy, required no peak-overlap corrections. The present method for EMPA of *REE*, except for Nd, has been developed from that adopted by Wing *et al*. (2003).

Elements detected with qualitative analyses were measured by quantitative analyses. Allanite grains were analysed quantitatively for major elements (Si, Ti, Al, Fe, Zn, Mn, Mg, Ca, Th) at a voltage of 25 kV, beam current of 10 nA, and

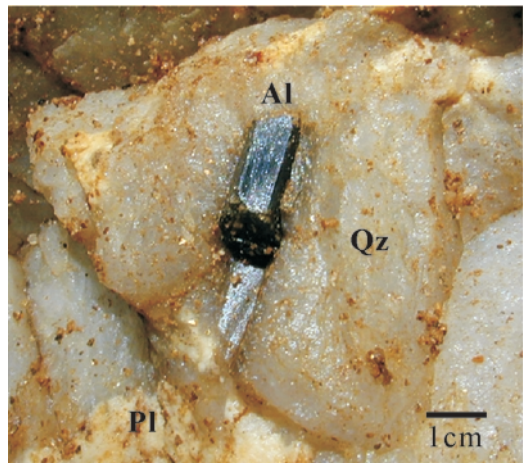

FIG. 2. Photograph of the unaltered and non-metamict allanite crystal included in quartz in granitic pegmatite from the Daibosatsu Pass. Al: allanite; Qz: quartz; Pl: plagioclase.

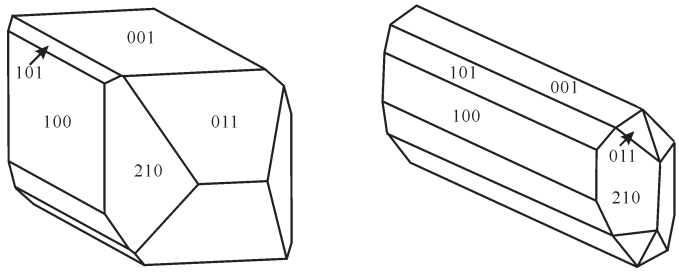

FIG. 3. Morphology of allanites from (*a*) island arc and (*b*) intracontinental settings.

TABLE 1. Standard materials used for wavelength dispersive electron microprobe analysis.

Standard element	Chemical composition (wt.%)
Si	SiO_2 (100.0)
Ti	TiO_2 (100.0)
Th	ThO_2 (100.0)
Al	Al_2O_3 (100.0)
Fe	Fe_2O_3 (100.0)
Zn	SiO_2 (33.11), ZnO (66.89)
Mn	MnO (30.76), Fe_2O_3 (69.24)
Mg	MgO (100.0)
Ca	SiO_2 (51.73), CaO (48.27)
Y	SiO_2 (54.3), Al_2O_3 (12.7), CaO (20.5), Y_2O_3 (11.8)
La	SiO_2 (54.3), Al_2O_3 (12.7), CaO (20.6), La_2O_3 (11.5)
Ce	SiO_2 (54.2), Al_2O_3 (12.8), CaO (20.4), Ce_2O_3 (11.9)
Pr	SiO_2 (54.0), Al_2O_3 (12.7), CaO (20.6), Pr_2O_3 (12.2)
Nd	SiO_2 (54.4), Al_2O_3 (12.8), CaO (20.8), Nd_2O_3 (11.8)
Sm	SiO_2 (54.8), Al_2O_3 (12.9), CaO (20.8), Sm_2O_3 (11.2)
Gd	SiO_2 (54.8), Al_2O_3 (12.1), CaO (20.7), Gd_2O_3 (12.1)
Dy	SiO_2 (54.7), Al_2O_3 (12.5), CaO (20.6), Dy_2O_3 (12.0)

count times of 20 s. Concentrations of *REE* were measured at 25 kV with a 50 nA beam current, and count times of 20 s. Both beam currents were corrected with the following:

$$K = \frac{\text{Intensity (specimen)}}{\text{Intensity (standard)}} \times \frac{\text{Beam current (standard)}}{\text{Beam current (specimen)}} \times \text{composition (standard)}$$

There were two types of measurement for the present analyses because the analytical error would be great if all elements were analysed at the same beam current (Uchiyama *et al*., 1972); a list of the standards used in this study is presented in Table 1; and all data were corrected with a 'ZAF' matrix-correction program.

X-ray powder diffraction

The degrees of metamictization for allanites were examined by X-ray powder diffraction (PXRD) analysis. Samples were X-rayed with Cu-$K\alpha_1$ radiation (40 kV, 30 mA) using a Rigaku Geigerflex system with a flat graphite monochromator and 1° divergence slit. Whole patterns from 5 to 65°2θ were scanned at 0.1°2θ steps and the reflections in the 24.5–26.0 and 30.0–31.5°2θ ranges at 0.01°2θ steps. The allanite samples were ground in an agate pestle until their powders were judged to be of a sufficiently small grain size to

TABLE 2. Details of data collection and refinement of allanite from the Daibosatsu Pass.

Diffractometer	Enraf-Nonius CAD4
Wavelength	Mo-$K\alpha$ radiation (λ = 0.71069 Å)
Temperature	296 K
Crystal size	0.1 × 0.1 × 0.1 mm
Scan mode	ω/2θ
a	8.905(1) Å
b	5.7606(5) Å
c	10.123(1) Å
β	114.78(1)°
V	470.7(2) Å^3
Space group	$P2_1/m$
Z	2
$2\theta_{max}$	70
Total reflections	5557
Unique reflections	1498
R_{int} value	0.01
Unique $F_0 > 4\sigma(F_0)$	1459
$F(000)$	549.5
R value	3.46%
*R*w value	10.49%
Goodness of fit	1.28
μ	7.87 mm^{-1}

TABLE 3. Atomic coordinates and equivalent displacement parameters (Å^2).

Atom	x	y	z	U_{eq}	U_{11}	U_{22}	U_{33}	U_{23}	U_{13}	U_{12}
*A*1	0.7585(2)	0.75	0.1515(2)	0.0219(4)	0.0272(9)	0.0190(8)	0.0221(8)	−0	0.0128(7)	−0
*A*2	0.59375(6)	0.75	0.42924(5)	0.0233(3)	0.0215(3)	0.0254(3)	0.0216(3)	−0	0.0075(2)	−0
*M*1	0	0	0	0.0246(4)	0.0231(8)	0.0238(9)	0.0260(8)	−0.0002(6)	0.0094(6)	0.0003(6)
*M*2	0	0	0.5	0.0206(5)	0.0184(9)	0.019(1)	0.024(1)	−0.0007(8)	0.0083(8)	0.0009(8)
*M*3	0.3030(1)	0.25	0.2135(1)	0.0245(3)	0.0211(6)	0.0237(6)	0.0257(6)	−0	0.0069(5)	−0
Si1	0.3386(2)	0.75	0.0359(2)	0.0214(4)	0.020(1)	0.021(1)	0.022(1)	−0	0.0067(8)	−0
Si2	0.6866(2)	0.25	0.2798(2)	0.0216(4)	0.020(1)	0.021(1)	0.023(1)	−0	0.0076(8)	−0
Si3	0.1886(2)	0.75	0.3245(2)	0.0210(4)	0.0189(9)	0.021(1)	0.021 (1)	−0	0.0066(7)	−0
O1	0.2330(5)	0.9877(8)	0.0245(5)	0.0268(8)	0.023(1)	0.021(1)	0.035(2)	−0.001(1)	0.010(1)	−0.000(1)
O2	0.3135(5)	0.9718(8)	0.3653(5)	0.0243(7)	0.023(1)	0.024(1)	0.025(1)	−0.001(1)	0.009(1)	−0.004(1)
O3	0.7966(5)	0.0147(7)	0.3381(4)	0.0264(8)	0.024(1)	0.021(1)	0.029(2)	−0.001(1)	0.006(1)	−0.001(1)
O4	0.0565(8)	0.25	0.1292(7)	0.025(1)	0.022(2)	0.026(2)	0.026(2)	−0	0.009(2)	−0
O5	0.0496(8)	0.75	0.1518(6)	0.025(1)	0.026(2)	0.027(2)	0.019(2)	−0	0.008(2)	−0
O6	0.0675(8)	0.75	0.4118(6)	0.024(1)	0.025(2)	0.021(2)	0.026(2)	−0	0.011(2)	−0
O7	0.5095(8)	0.75	0.1788(7)	0.028(1)	0.026(2)	0.025(2)	0.029(3)	−0	0.007(2)	−0
O8	0.5413(8)	0.25	0.3355(7)	0.033(1)	0.026(2)	0.048(4)	0.027(3)	−0	0.014(2)	−0
O9	0.6084(8)	0.25	0.1015(6)	0.028(1)	0.030(2)	0.038(3)	0.016(2)	−0	0.010(2)	−0
O10	0.0851(7)	0.25	0.4280(6)	0.024(1)	0.024(2)	0.022(1)	0.025(3)	−0	0.010(2)	−0

Site contents: $(Ca_{0.92}\square_{0.080})_{\Sigma 1.000}$ for *A*1, $(La_{0.238}Ce_{0.443}Pr_{0.048}Nd_{0.100}Sm_{0.019}Th_{0.042}Mn_{0.008}\square_{0.102})_{\Sigma 1.000}$ for *A*2, $(Al_{0.607}Fe^{3+}_{0.317}Ti_{0.076})_{\Sigma 1.000}$ for *M*1, $(Al_{1.000})_{\Sigma 1.000}$ for *M*2 and $(Fe^{2+}_{0.543}Fe^{3+}_{0.365}Mn_{0.055}Mg_{0.037})_{\Sigma 1.000}$ for *M*3.

TABLE 4. Bond lengths (Å) and angles (°).

*A*1–O3 × 2[ab]	2.339(4)	*M*1–O4 × 2[j]	1.867(4)
O7	2.347(4)	O1 × 2[kl]	1.985(4)
O1 × 2[cd]	2.361(5)	O5 × 2[kl]	2.015(4)
O5[e]	2.591(7)	Mean	1.956
O6[e]	2.905(7)		
O9 × 2[a]	3.126(3)		
Mean	2.611		
		*M*2–O3 × 2[mn]	1.867(4)
		O10 × 2[0]	1.909(3)
		O6 × 2[kp]	1.919(4)
*A*2–O7	2.323(7)	Mean	1.898
O2 × 2[fg]	2.477(4)		
O10[h]	2.608(6)		
O2 × 2[i]	2.631(4)		
O3 × 2	2.799(4)	*M*3–O8	1.957(7)
O8 × 2	3.007(2)	O4	1.994(6)
Mean	2.676	O2 × 2[ik]	2.195(4)
		O1 × 2[ik]	2.309(5)
		Mean	2.160
Si1–O7	1.601(6)	O1–Si1–O7 × 2	111.3(2)
O1 × 2[i]	1.638(5)	O1–Si1–O1	113.5(3)
O9[q]	1.645(7)	O1–Si1–O9 × 2	107.5(2)
Mean	1.631	O7–Si1–O9	105.3(3)
Si2–O8	1.614(7)	O3–Si2–O8 × 2	108.8(2)
O3 × 2[b]	1.631(4)	O3–Si2–O3	112.4(3)
O9	1.640(7)	O9–Si2–O8	110.6(3)
Mean	1.629	O9–Si2–O3 × 2	108.2(2)
Si3–O2 × 2[i]	1.630(4)	O2–Si3–O2	103.3(3)
O6	1.656(6)	O6–Si3–O2 × 2	113.1(2)
O5	1.666(7)	O5–Si3–O2 × 2	113.2(2)
Mean	1.646	O5–Si3–O6	101.3(3)

Symmetry transformations used to generate equivalent atoms; [a] $x, y+1, z$; [b] $x, -y+½, z$; [c] $-x+1, y-½, -z$; [d] $-x+1, -y+2, -z$; [d] $x+1, y, z$; [f] $-x+1, -y+2, -z+1$; [g] $-x+1, y-½, -z+1$; [h] $-x+1, -y+1, -z+1$; [i] $x, -y+⅔, z$; [j] $-x, -y, -z$; [k] $x, y-1, z$; [l] $-x, -y+1, -z$; [m] $-x+1, -y, -z+1$; [n] $x-1, y, z$; [o] $-x, -y, -z+1$; [p] $-x, -y+1, -z+1$; [q] $-x+1, -y+1, -z$.

avoid problems associated with micro-absorption. Silicon metal powder was used as an angle-calibration internal standard for angle diffraction. Each mixture of allanite sample (3 g) and silicon powder standard (0.333 g) was applied to the no-reflection quartz plate.

Fourier-transform infrared microspectroscopy

The (OH^-) presence and metamictization in allanites were confirmed by Janssen Micro Fourier-transform infrared spectroscopy (FTIR; Jasco, Inc.). Single crystals of allanite, 20 μm thick, were chosen under a stereomicroscope and placed on a KBr plate. Each spectrum was measured in the 650–4000 cm^{-1} region, with a 1 cm^{-1} resolution.

Single crystal X-ray intensity measurement

Single crystal X-ray-diffraction intensities for the Daibosatsu allanite-(Ce) were collected with an automated diffractometer (CAD4; Enraf-Nonius B.V.) with graphite-monochromated Mo-$K\alpha$ radiation from an irregular fragment of dimensions $0.1 \times 0.1 \times 0.1$ mm. Twenty reflections within the range $20° \leqslant 2\theta \leqslant 30°$ were centred such that unit-cell dimensions (Table 2) could be

TABLE 5. Empirical bond valence (v.u.)*.

	*A*1	*A*2	*M*1	*M*2	*M*3	Si1	Si2	Si3	H	Σv.u.
O1	$\downarrow^{\times 2}0.32\rightarrow$		$\downarrow^{\times 2}0.45^{\rightarrow}$		$\downarrow^{\times 2}0.22^{\rightarrow}$	$\downarrow^{\times 2}0.96^{\rightarrow}$				1.95
O2		$\downarrow^{\times 2}0.32^{\rightarrow}$			$\downarrow^{\times 2}0.30^{\rightarrow}$			$\downarrow^{\times 2}0.98^{\rightarrow}$		1.81
		$\downarrow^{\times 2}0.21^{\rightarrow}$								
O3	$\downarrow^{\times 2}0.34\rightarrow$	$\downarrow^{\times 2}0.13^{\rightarrow}$		$\downarrow^{\times 2}0.56^{\rightarrow}$			$\downarrow^{\times 2}0.98^{\rightarrow}$			2.01
O4			$\downarrow^{\times 2}0.62^{\times 2\rightarrow}$		$\downarrow 0.51^{\rightarrow}$				0.25	2.00
O5	$\downarrow 0.17\rightarrow$		$\downarrow^{\times 2}0.41^{\times 2\rightarrow}$					$\downarrow 0.89^{\rightarrow}$		1.88
O6	$\downarrow 0.07\rightarrow$							$\downarrow 0.92^{\rightarrow}$		1.95
O7	$\downarrow 0.33\rightarrow$	$\downarrow 0.48^{\rightarrow}$				$\downarrow 1.07^{\rightarrow}$				1.88
O8		$\downarrow^{\times 2}0.08^{\times 2\rightarrow}$	$\downarrow^{\times 2}0.48^{\times 2\rightarrow}$		$\downarrow 0.56^{\rightarrow}$		$\downarrow 1.03^{\rightarrow}$			1.75
O9	$\downarrow^{\times 2}0.04^{\times 2\rightarrow}$					$\downarrow 0.95^{\rightarrow}$	$\downarrow 0.96^{\rightarrow}$			1.99
O10		$\downarrow 0.22^{\rightarrow}$		$\downarrow^{\times 2}0.50^{\times 2\rightarrow}$					0.75	1.97
Σva	1.97	2.18	2.96	3.08	2.11	3.94	3.95	3.77	1.00	

* The bond-valence constants are from Brese and O'Keefe (1991). Bond-valence sums are weighted by the atomic ratio for $(Ca_{0.92}\square_{0.080})_{\Sigma 1.000}$ for *A*1, $(La_{0.238}Ce_{0.443}Pr_{0.048}Nd_{0.100}\ Sm_{0.019}Th_{0.042}Mn_{0.008}\square_{0.102})_{\Sigma 1.000}$ for *A*2, $(Al_{0.607}Fe^{3+}_{0.317}Ti_{0.076})_{\Sigma 1.000}$ for *M*1, $(Al_{1.000})_{\Sigma 1.000}$ for *M*2 and $(Fe^{2+}_{0.543}Fe^{3+}_{0.365}Mn_{0.055}Mg_{0.037})_{\Sigma 1.000}$ for *M*3, respectively. The bond valence of the H atom was assigned to be in accordance with the incident bond-valence requirements of the O4 and O10 atoms.

TABLE 6. Electron microprobe analysis (mean and standard deviation of 7 points) of allanite from the Daibosatsu Pass used for the structure refinement. Unit formulae normalized to12.5 oxygens.

Oxide (wt.%)	mean	s.d.	a.p.f.u.	mean	s.d.
SiO_2	30.49	0.02	Si	3.000	0.004
TiO_2	1.06	0.03	Ti	0.076	0.007
ThO_2	1.91	0.01	Th	0.042	0.005
Al_2O_3	14.27	0.02	Al	1.607	0.005
Fe_2O_3	9.00	0.02	Fe^{3+}	0.682	0.006
La_2O_3	6.74	0.02	La	0.238	0.005
Ce_2O_3	13.28	0.03	Ce	0.443	0.005
Pr_2O_3	1.39	0.05	Pr	0.048	0.008
Nd_2O_3	2.93	0.01	Nd	0.100	0.003
Sm_2O_3	0.59	0.05	Sm	0.019	0.007
FeO	7.16	0.02	Fe^{2+}	0.543	0.006
MnO	0.78	0.04	Mn	0.063	0.006
MgO	0.26	0.02	Mg	0.037	0.005
CaO	8.99	0.02	Ca	0.920	0.005
Total	98.85	0.03	Total	7.818	0.006

Chemical formula:
$(Ca_{0.920}\square_{0.080})_{\Sigma 1.000}(La_{0.238}Ce_{0.443}Pr_{0.048}Nd_{0.100}Sm_{0.019}Th_{0.042}Mn_{0.008}\square_{0.102})_{\Sigma 1.000}$
$(Al_{0.607}Fe^{3+}_{0.317}Ti_{0.076})_{\Sigma 1.000}(Al_{1.000})(Fe^{2+}_{0.543}Fe^{3+}_{0.365}Mn_{0.055}Mg_{0.037})_{\Sigma 1.000}(SiO_4)(Si_2O_7)O(OH)$.
$\square$ stands for a defect.

refined by least-squares from the resultant setting angles. Intensity data were collected in ω-2θ scan-mode at a fixed scan-rate of 1.0º2θ/ min. In all, 5557 reflections were measured within the range of $4^\circ \leqslant 2\theta \leqslant 60^\circ$. Psi-scan data were measured on five reflections at increments of 10º about the diffraction vector; absorption correction was applied using the semi-empirical method (North *et al*., 1968). Data were corrected for Lorentz, polarization and background effects, averaged and reduced to structure factors. The resultant 1459 unique reflections were considered as observed [$F_0 = 4\sigma(F_0)$]. Final atomic positional and equivalent displacement parameters are given in Table 3. Table 4 shows selected interatomic distances and angles. Table 5 presents bond valence analysis.

Results

Chemical composition

The present EMPA demonstrates that Ce is predominant over other *REE* in all analysed allanite grains from the Daibosatsu Pass, which were identified as allanite-(Ce) (Table 6). This allanite is characterized by a narrow range of compositional variation and its chemical zoning escapes EMPA detection. For calculation of Fe^{2+}/Fe^{3+} in allanite formula, Ercit (2002) has suggested that the method based on 6 (M + T) cations and 12 (O) + 1(OH) per formula is superior. However, his calculation of the allanite formula was suggested based on the chemical compositions before establishment of the improved EMPA method for accurate *REE* detection (Reed and Buckley, 1998; Nishida *et al*., 1999). Thus it is assumed that Si is 3 as a basis of normalization, which has been applied in crystal structure refinements of *REE*-bearing epidote group minerals (Dollase, 1971; Peacor and Dunn, 1988; Rouse and Peacor, 1993). Therefore, structural formulae were calculated based on 12.5 oxygens, after normalization of chemical data to 3 Si atoms per formula unit. Table 6 lists assignments of cations based on charge balance. Allanites from granitic rocks of Haguri, Omiyadani, Daian, Suishoyama, Fukudayama and Shimo-ono in Japan, were also analysed by EMPA. The location of these samples are shown in Fig. 1. All of these allanites proved to be of a Ce type. Tables 7 and 8 list chemical compositions of these allanites in comparison with that of the refined allanite from the Daibosatsu Pass (Table 6).

TABLE 7. Electron microprobe analysis (mean and standard deviation of 10 points) of allanites from Haguri, Omiyadani and Daian in Japan. Unit formulae normalized to 12.5 oxygens.

Oxide (wt.%)	Haguri-D		Haguri-B		Omiyadani-D		Omiyadani-B		Daian-D		Daian-B	
	mean	s.d.	mean	s.d	mean	s.d.	mean	s.d.	mean	s.d.	mean	s.d.
SiO_2	31.44	0.05	31.23	0.07	33.48	0.05	33.77	0.03	32.30	0.03	32.14	0.05
TiO_2	0.00	0.00	0.00	0.00	1.16	0.02	0.42	0.05	1.57	0.02	1.49	0.07
ThO_2	1.76	0.07	1.48	0.04	1.13	0.04	1.26	0.02	3.60	0.01	3.20	0.05
Al_2O_3	15.96	0.05	15.83	0.03	17.73	0.04	17.72	0.03	16.73	0.04	15.32	0.04
Fe_2O_3	8.51	0.08	8.70	0.05	6.55	0.03	7.27	0.03	7.25	0.05	7.46	0.02
Y_2O_3	1.93	0.04	1.90	0.01	0.00	0.00	0.00	0.00	0.75	0.03	0.91	0.03
La_2O_3	2.28	0.03	2.26	0.02	5.89	0.07	5.99	0.06	4.44	0.02	5.02	0.04
Ce_2O_3	6.65	0.02	6.66	0.02	8.33	0.05	8.74	0.05	7.82	0.04	8.08	0.04
Pr_2O_3	1.48	0.03	1.52	0.03	1.16	0.05	1.19	0.08	1.32	0.04	1.37	0.02
Nd_2O_3	6.20	0.04	6.26	0.02	3.43	0.04	4.02	0.05	3.98	0.05	4.31	0.01
Sm_2O_3	2.87	0.02	2.88	0.04	0.50	0.02	0.54	0.04	0.98	0.02	0.17	0.05
Gd_2O_3	2.08	0.05	2.21	0.05	1.02	0.03	1.05	0.04	1.01	0.01	1.06	0.04
Dy_2O_3	0.86	0.03	0.84	0.03	0.00	0.00	0.00	0.00	0.52	0.01	0.61	0.02
FeO	7.83	0.08	8.25	0.02	6.12	0.03	6.82	0.03	6.71	0.05	6.75	0.02
ZnO	0.00	0.00	0.00	0.00	0.53	0.04	0.32	0.04	0.00	0.00	0.00	0.00
MnO	6.61	0.04	7.31	0.05	0.54	0.05	0.65	0.02	1.01	0.04	1.05	0.01
MgO	0.00	0.00	0.00	0.00	0.85	0.04	0.50	0.04	0.46	0.03	0.55	0.04
CaO	3.13	0.04	2.33	0.01	11.21	0.03	9.81	0.05	7.88	0.04	9.31	0.04
Total	99.58	0.05	99.66	0.03	99.63	0.04	99.29	0.04	98.33	0.03	98.80	0.04

Allanites from Haguri, Omiyadani and Daian have two kinds of dark (D) and light (B) domains, observed on the backscattered electron image.

Chemical formula

Haguri-D:

$(Ca_{0.321}Mn_{0.536}\square_{0.143})_{\Sigma 1.000}(Y_{0.098}La_{0.081}Ce_{0.233}Pr_{0.052}Nd_{0.212}Sm_{0.095}Gd_{0.066}Dy_{0.026}Th_{0.038}Fe^{2+}_{0.046}\square_{0.053})_{\Sigma 1.000}$
$(Al_{0.803}Fe^{3+}_{0.197})_{\Sigma 1.000}(Al_{1.000})(Fe^{2+}_{0.550}Fe^{3+}_{0.450})_{\Sigma 1.000}\ (SiO_4)(Si_2O_7)\ O(OH).$

Haguri-B:

$(Ca_{0.239}Mn_{0.595}\square_{0.166})_{\Sigma 1.000}(Y_{0.097}La_{0.080}Ce_{0.235}Pr_{0.053}Nd_{0.215}Sm_{0.095}Gd_{0.070}Dy_{0.026}Th_{0.032}Fe^{2+}_{0.085}\square_{0.012})_{\Sigma 1.000}$
$(Al_{0.793}Fe^{3+}_{0.207})(Al_{1.000})(Fe^{2+}_{0.585}Fe^{3+}_{0.415})_{\Sigma 1.000}\ (SiO_4)(Si_2O_7)\ O(OH).$

Omiyadani-D:

$(Ca_{1.000})(La_{0.195}Ce_{0.261}Pr_{0.038}Nd_{0.110}Sm_{0.015}Gd_{0.030}Th_{0.023}Ca_{0.076}Fe^{2+}_{0.040}\square_{0.212})_{\Sigma 1.000}(Al_{0.873}Ti_{0.078}Fe^{3+}_{0.049})_{\Sigma 1.000}$
$(Al_{1.000})_{\Sigma 1.000}(Fe^{2+}_{0.418}Fe^{3+}_{0.393}Mg_{0.113}Mn_{0.041}Zn_{0.035})_{\Sigma 1.000}\ (SiO_4)(Si_2O_7)\ O(OH).$

Omiyadani-B:

$(Ca_{0.955}\square_{0.045})_{\Sigma 1.000}(La_{0.201}Ce_{0.277}Pr_{0.039}Nd_{0.131}Sm_{0.017}Gd_{0.032}Th_{0.026}Fe^{2+}_{0.082}\square_{0.044})_{\Sigma 1.000}$
$(Al_{0.899}Fe^{3+}_{0.072}Ti_{0.029})_{\Sigma 1.000}(Al_{1.000})(Fe^{2+}_{0.436}Fe^{3+}_{0.425}Mg_{0.068}Mn_{0.050}Zn_{0.021})_{\Sigma 1.000}(SiO_4)(Si_2O_7)\ O(OH).$

Daian-D:

$(Ca_{0.784}\square_{0.216})_{\Sigma 1.000}(Y_{0.037}La_{0.152}Ce_{0.254}Pr_{0.045}Nd_{0.132}Sm_{0.031}Gd_{0.031}Dy_{0.016}Th_{0.076}Fe^{2+}_{0.112}\square_{0.114})_{\Sigma 1.000}$
$(Al_{0.831}Ti_{0.110}Fe^{3+}_{0.059})_{\Sigma 1.000}(Al_{1.000})(Fe^{3+}_{0.448}Fe^{2+}_{0.409}Mn_{0.079}Mg_{0.064})_{\Sigma 1.000}(SiO_4)(Si_2O_7)\ O(OH).$

Daian-B:

$(Ca_{0.931}\square_{0.069})_{\Sigma 1.000}(Y_{0.045}La_{0.173}Ce_{0.263}Pr_{0.047}Nd_{0.144}Sm_{0.005}Gd_{0.033}Dy_{0.018}Th_{0.068}Fe^{2+}_{0.001}\square_{0.203})_{\Sigma 1.000}$
$(Al_{0.685}Fe^{3+}_{0.210}Ti_{0.105})_{\Sigma 1.000}(Al_{1.000})(Fe^{2+}_{0.526}Fe^{3+}_{0.314}Mn_{0.083}Mg_{0.077})_{\Sigma 1.000}\ (SiO_4)(Si_2O_7)\ O(OH).$

$\square$ stands for a defect.

The present allanites have only moderate Mn contents, but the allanites from Haguri and Suishoyama have appreciable Mn contents (~7 wt.% MnO), equivalent to manganoan allanite containing 6.74 wt.% of MnO (Hutton, 1951). Moreover, ThO_2 contents in the analysed allanites are in the range 1.13–3.60 wt.% (Tables 6, 7 and 8), approximately consistent with the compiled data for chemical compositions of allanite (Gieré and Sorensen, 2004). This incorporation contrasts with variations in Th content between grains within a single thin section of allanite in granite from Japan (Hayase, 1954). However the mechanisms of

TABLE 8. Electron microprobe analysis (mean and standard deviation of 10 points) of allanites from Suishoyama, Fukudayama and Shimo-ono in Japan. Unit formulae normalized to12.5 oxygens.

Oxide (wt.%)	Suishoyama		Fukudayama		Shimo-ono	
	mean	s.d.	mean	s.d.	mean	s.d.
SiO_2	30.54	0.06	32.11	0.17	31.37	0.27
TiO_2	0.00	0.00	0.00	0.00	1.40	0.02
ThO_2	1.17	0.04	2.81	0.03	3.43	0.09
Al_2O_3	13.55	0.05	16.36	0.12	13.66	0.10
Fe_2O_3	8.47	0.04	8.55	0.06	7.96	0.11
Sc_2O_3	0.19	0.01	0.24	0.00	0.00	0.00
Y_2O_3	1.36	0.09	2.77	0.04	1.45	0.04
La_2O_3	3.62	0.13	2.14	0.05	2.32	0.07
Ce_2O_3	8.36	0.14	4.68	0.12	5.37	0.17
Pr_2O_3	1.79	0.03	1.21	0.02	1.45	0.03
Nd_2O_3	5.51	0.05	4.22	0.04	5.67	0.05
Sm_2O_3	1.97	0.04	2.45	0.05	2.25	0.04
Gd_2O_3	1.56	0.06	2.55	0.01	1.91	0.02
Dy_2O_3	1.10	0.02	1.55	0.04	1.08	0.04
FeO	7.96	0.04	7.53	0.06	8.32	0.11
MnO	6.70	0.18	2.83	0.04	3.92	0.05
MgO	0.00	0.00	0.00	0.00	0.27	0.00
CaO	4.81	0.11	7.43	0.04	7.82	0.06
Total	98.66	0.19	99.43	0.35	99.65	0.61

Chemical formula
Suishoyama:
$(Ca_{0.508}Mn_{0.421})_{\Sigma 1.000}(Sc_{0.016}Y_{0.072}La_{0.132}Ce_{0.302}Pr_{0.064}Nd_{0.194}Sm_{0.067}Gd_{0.051}Dy_{0.035}Th_{0.026}\square_{0.042})_{\Sigma 1.000}$
$(Al_{0.575}Fe^{3+}_{0.425})_{\Sigma 1.000}(Al_{1.000})(Fe^{2+}_{0.623}Fe^{3+}_{0.238}Mn_{0.139})_{\Sigma 1.000}$ $(SiO_4)(Si_2O_7)$ O(OH).
Fukudayama:
$(Ca_{0.748}Mn_{0.225}\square_{0.027})_{\Sigma 1.000}(Sc_{0.02}Y_{0.139}La_{0.074}Ce_{0.161}Pr_{0.041}Nd_{0.142}Sm_{0.079}Gd_{0.079}Dy_{0.047}Th_{0.060}$
$Fe^{2+}_{0.010}\square_{0.148})_{\Sigma 1.000}(Al_{0.793}Fe^{3+}_{0.207})_{\Sigma 1.000}(Al_{1.000})(Fe^{2+}_{0.585}Fe^{3+}_{0.415}Mn_{0.082}Mg_{0.038})_{\Sigma 1.000}$ $(SiO_4)(Si_2O_7)$ O(OH).
Shimo-ono:
$(Ca_{0.803}Mn_{0.197})_{\Sigma 1.000}(Y_{0.074}La_{0.082}Ce_{0.188}Pr_{0.051}Nd_{0.194}Sm_{0.074}Gd_{0.061}Dy_{0.033}Th_{0.075}Mn_{0.039}\square_{0.129})_{\Sigma 1.000}$
$(Al_{0.542}Fe^{3+}_{0.357}Ti_{0.101})_{\Sigma 1.000}(Al_{1.000})(Fe^{2+}_{0.632}Fe^{3+}_{0.248}Mn_{0.082}Mg_{0.038})_{\Sigma 1.000}$ $(SiO_4)(Si_2O_7)O(OH)$.
$\square$ stands for a defect.

coupled substitutions responsible for Th incorporation are complex and speculative (Gieré and Sorensen, 2004). The most distinctive feature of allanites from granitic rocks of the Japanese island arc is that no U was detected by EMPA even though Th is present in all the samples. Deer *et al.* (1986) did suggest that Th and U are present in the majority of allanites. However some reports (e.g. Hasegawa, 1960; Suzuki *et al.*, 1990) concluded that allanites from granitic rocks in Japan often contain less than 0.1% U. Th-U partitioning between allanite and melt (or solution) will be discussed in more detail later.

X-ray powder diffraction

Intensities of two X-ray powder diffraction lines, $I(21\bar{1})$ and $I(11\bar{3})$, for allanites from the Daibosatsu Pass, Suishoyama, Fukudayama and Shimo-ono, respectively, are compared in Table 9 and Fig. 4. The process of metamictization of allanite greatly influences intensities and *d* spacings of its X-ray powder diffraction lines (e.g. Ueda, 1957; Pellas, 1961). With decreasing degree of lattice ordering, diffraction peaks appear to become less intense and less sharp. As is evident from Table 9 and Fig. 4, with increasing amorphization, the XRD peaks decrease in both sharpness and intensity, but their shift towards lower 2θ (i.e. larger *d* spacings) is not distinctive because of the variety of chemical composition of the investigated allanites, and finally they fade away: the degree of metamictization increases in the order: Daibosatsu Pass, Suishoyama, Fukudayama and Shimo-ono. Moreover, clay minerals were not

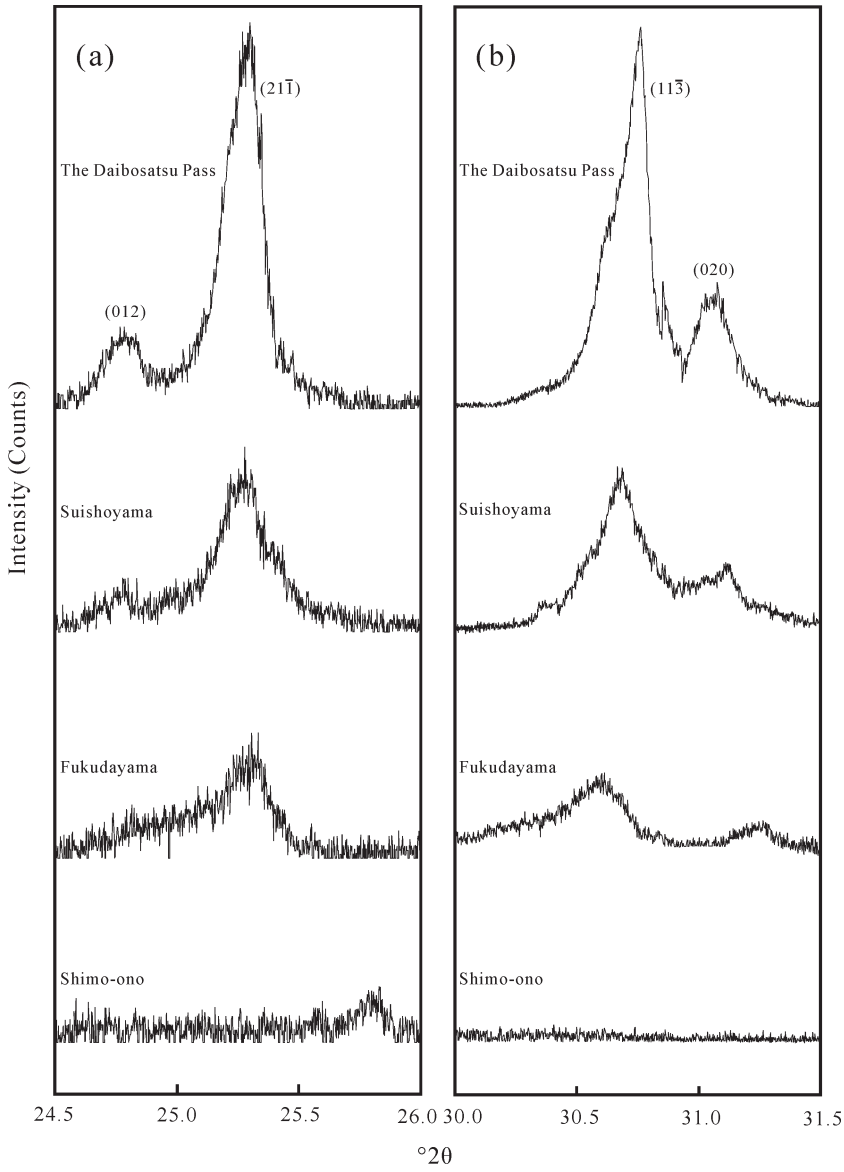

FIG. 4. PXRD patterns of four allanites (Daibosatsu Pass, Suishoyama, Fukudayama and Shimo-ono) representing the 2θ ranges suggestive of radiation damage, from well crystallized to fully metamict states. (*a*) Profiles of (21$\bar{1}$) peak. (*b*) Profiles of (11$\bar{3}$) peak.

detected in these allanites, which shows that these allanites were not altered. Therefore, the decrease in crystallinity of the examined allanites is found to result from metamictization only. Therefore, the Daibosatsu allanite is a suitable sample for crystal structure refinement.

Fourier-transform infrared microspectroscopy

The (OH^-) spectrum of unaltered and non-metamict allanite from the Daibosatsu Pass consists of two main stretching bands at 3187 cm^{-1} and 3355 cm^{-1} (Fig. 5). This observation entirely conforms with the OH-stretching

TABLE 9. The *d* spacing, full width at half maximum (FWHM) intensity and intensity for Bragg and diffuse scattering components of the $(21\bar{1})$ and $(11\bar{3})$ reflections of allanites from granitic pegmatites in Japan.

Sample	*d* (Å)	FWHM (°2θ)	Intensity (counts/mg)*
		$21\bar{1}$ reflection	
Daibosatsu Pass	3.516	0.149	37.6
Suisyoyama	3.520	0.236	12.0
Fukudayama	3.515	0.247	7.6
Shimo-ono	n.d.**	n.d.	n.d.
		$11\bar{3}$ reflection	
Daibosatsu Pass	2.905	0.186	85.6
Suisyoyama	2.912	0.278	33.6
Fukudayama	2.916	0.321	13.6
Shimo-ono	n.d.	n.d.	n.d.

* Intensity of investigated allanites is normalized to the amount of sample mounted on an X-ray non-reflection quartz holder.
** n.d.: not detected.

bands in epidote (Čech *et al*., 1972). On the other hand, the spectra of metamict allanites from granitic rocks from Suishoyama, Fukudayama and Shimo-ono show relatively broad absorption peaks at ~3225, 3218 and 3209 cm^{-1}, respectively (Fig. 5), very different from those in the Daibosatsu allanite. In addition, the SiO-stretching band at 1035 cm^{-1} of the Daibosatsu allanite shifted towards the lower wavenumbers (~1021, 1017 and 1004 cm^{-1}) with the increasing metamict state characteristic of the other allanites (Fig. 5). Similar shifts were observed in the corresponding spectra of allanite, zircon and their metamict equivalents (Janeczek and Eby, 1993; Zhang and Salje, 2001). Therefore, the OH- and SiO-stretching bands may serve as indicators of metamictization.

Structure refinement

The program SHELXL-97 (Sheldrick, 1997) was used throughout this work. Refinement of the present structure under the constraints of the chemical composition, which is significantly different from that established by Dollase (1971), was carried out in the space group $P2_1/m$, with structural parameters given by Dollase (1971). Refinement of the positional parameters and isotropic displacement parameters converged to an *R* index of 3.84%. The anisotropic displacement model, together with refinement of all parameters, suggested an *R* index of 3.46%. This stage of refinement led to calculation of a three-dimensional difference-Fourier map, where the hydrogen atom position was not determined.

Further refinement was carried out with only Si assigned to tetrahedral sites, as refined with only Si occupying three tetrahedral sites for epidote group minerals (e.g. Dollase, 1971; Rouse and Peacor, 1993; Bonazzi *et al*., 1996). Form factors for Ca and (*REE* + Th + Mn) were applied, respectively. Occupancies of Ca in A1 and (*REE* + Th + Mn) in *A*2 were refined together with coordinates and isotropic temperature factors to determine the distribution of Ca and (*REE* + Th + Mn) in *A*1 and *A*2 sites of allanite. Form factors for *M*1, *M*2 and *M*3 sites were modeled with $(0.607Al^{3+} + 0.317Fe^{3+} + 0.076Ti)$, Al^{3+} and $(0.543Fe^{2+} + 0.365Fe^{3+} + 0.055Mn + 0.037Mg)$, respectively, based on considerations of charge balance, the crystal-chemical data for other epidote group minerals (Dollase, 1971; Kvick *et al*., 1988; Rouse and Peacor, 1993), and known interatomic distances in allanites (Dollase, 1971). In particular, $A1^{3+}$ has a strong preference for *M*2 in epidote structures, whereas clarifying any ambiguity in the distribution of other cations through refinement is difficult because of the similarity in respective form factors of Al and Mg, and Fe and Mn. Therefore, cation-occupancies for *M*1 and *M*3 sites were fixed at the representative EMPA value (Table 6). For that reason, starting occupancy factors can be tested by comparing expected mean bond lengths for the

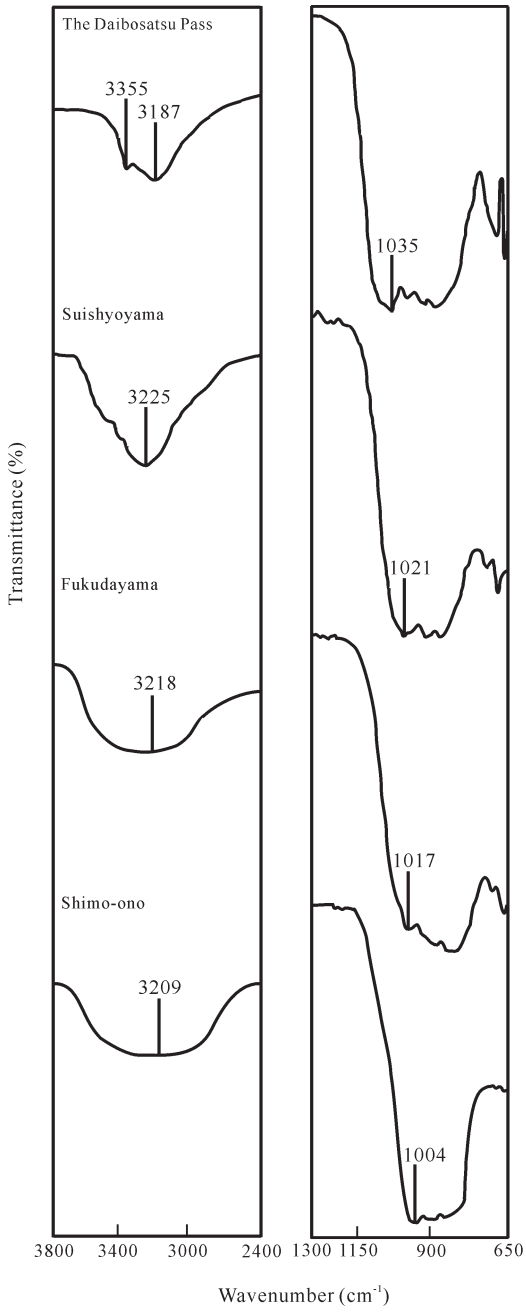

FIG. 5. IR data for non-metamict allanites from the Daibosatsu Pass, and for metamict allanites from Suishyoyama, Fukudayama and Shimo-ono.

M sites, calculated using the proportions of Al, Fe, Ti, Mn and Mg from the refinement and the mean of all measurements values for Al-O, Fe^{2+}-O, Fe^{3+}-O, Ti-O, Mn^{2+}-O and Mg-O from the survey of Baur (1981), with the observed mean bond lengths (Table 4). As shown in Table 10, similarity between the predicted and observed means is considered to be sufficient because differences in *M*1 and *M*2 sites are no more than ±0.01 Å. The error in measurements of bond lengths of the *M*3 site is larger than those of the *M*1 and *M*2 sites, and is considered to result from both the Jahn-Teller effect of Fe^{2+} in *M*3 site (Ksenofontov *et al*., 1985) and deformation of *M*3 polyhedra sharing edges with distorted *REE*-bearing *A*2 polyhedra (Fig. 6). Concerning the presence of vacancies (□) in the *A* sites, Peterson and MacFarlane (1993) reported the defect ranging from 0.05 to 0.40, while refinement of the crystal structure of khristovite-(Ce) (Sokolova *et al*., 1991) suggested that there are $□_{0.20}$ at the *A*1 site and $□_{0.07}$ at *A*2. All allanite grains analysed in this study also retain the defect in *A* sites ranging from 0.042 to 0.330 (Tables 6, 7 and 8). Besides, the result of the structural refinement for the present allanite sample from the Daibosatsu Pass showed that *A*1 and *A*2 sites have 0.080 and 0.102 vacancies, respectively. This model is supported by bond-valence considerations: greater charge cations (REE^{3+}, Th^{4+}) prefer *A*2, and the bond-valence contributions from the 9-coordinated cation at *A*1 to its coordinating anions are much less than those from the 10-coordinated cation at *A*2 (Table 5). Therefore, the vacancies at the *A*1 and *A*2 sites determined by the chemical composition and crystal structure refinement for the Daibosatsu allanite will find general acceptance with the crystal chemistry of allanite.

Discussion

Crystal chemistry of allanite

The coordination polyhedra are where *REE*s are known to be distorted in inorganic lanthanide

TABLE 10. Comparison between the mean bond lengths calculated and observed for *M* sites.

	Calculated	Observed
*M*1	1.95	1.96
*M*2	1.91	1.90
*M*3	2.09	2.16

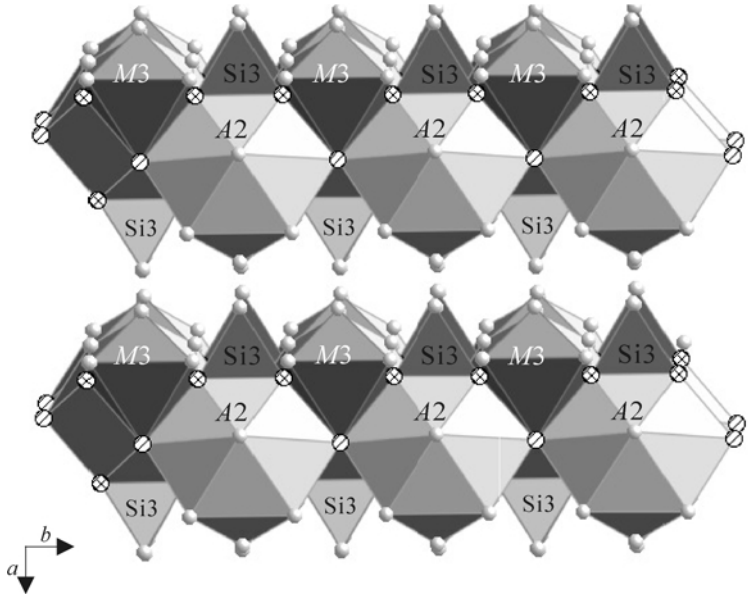

FIG. 6. The structure of epidote group minerals with edge sharing *A*2 polyhedra, *M*3 octahedra and Si3 tetrahedra by O2 and O8 atoms. O2 and O8 atoms are shown as ⊗ and ⊘, respectively. The other O atoms are shown as ○.

compounds with complex anions (Wickleder, 2002). In *REE*s, electrons are removed from the localized 4*f* state. According to the explanation by Burdett (1995), what happens is the creation of a small polaron, a region associated with a local geometrical distortion around the site where one *REE* atom has lost electrons. Therefore, in allanite the polyhedra with the *A*2 sites occupied by *REE* tend towards distortion.

The observation of $D_U/D_{Th} < 1$ (*D*: the bulk solid partition coefficients for U and Th) in allanite has often been reported (e.g. Oberli *et al*., 1981, 2004). The substitution mechanism responsible for Th incorporation in the present allanites (Tables 6, 7 and 8) can be explained by the following relation: $3Th^{4+} + \square$ (vacancy) $\rightleftharpoons 4REE^{3+}$, which was demonstrated in Fig. 7. This relationship means that crystal chemical properties of Th^{4+} and REE^{3+}cations harmonize with an *A*2 site in allanite. A site preference of Th^{4+} rather than U^{4+} in the allanite structure is considered to be due to large, *REE A*2 lattice sites, more favourable to the incorporation of the larger Th ion (1.05 Å in VIII-fold coordination) than U^{4+} (1.00 Å).

Tetrahedral distortions for SiO_4 and Si_2O_7 of epidote group minerals were calculated following the method of Robinson *et al*. (1971). Figure 6 illustrates the polyhedral linkage of three Si tetrahedra, *A*1 and *A*2 sites in the allanite structure. The observation that distortion of the Si3 tetrahedron is always the largest is common to epidote group minerals (Table 11). Dollase (1971) indicated that the Si3 tetrahedron is somewhat distorted probably due to the fact that

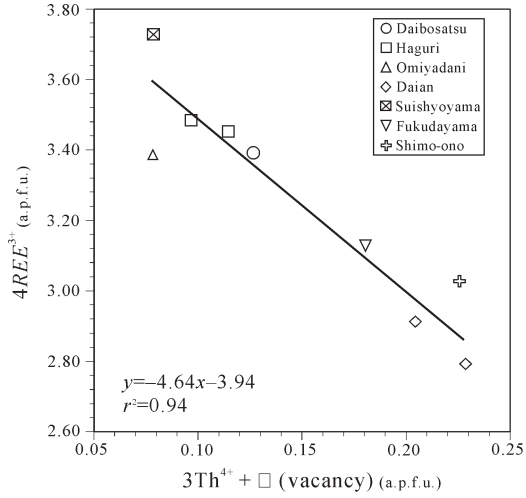

FIG. 7. Plot illustrating potential coupled substitution in allanite in granitic rocks from Japan. The composition of sample Omiyadani-D in Table 7 shows it is from a little-altered rim of a single allanite crystal. Therefore, the Omiyadani-D sample is not shown in Fig. 7.

TABLE 11. Tetrahedral distortions for Si_2O_7 (Si1 and Si2) and SiO_4 (Si3) of epidote group minerals calculated after Robinson *et al.* (1971)*.

	Epidote (Dollase, 1971)	Epidote (Gabe *et al.*, 1973)	Epidote (Kvick *et al.*, 1988)	Piemontite (Ferraris *et al.*, 1989)	Strontiopiemontite (Bonazzi *et al.*, 1990)	Hancockite (Dollase, 1971)	Dollaseite-(Ce) (Peacor and Dunn, 1988)
Si1	2.97	3.22	3.18	2.93	2.99	2.75	3.78
Si2	1.87	2.20	1.83	1.73	1.99	1.43	2.10
Si3	4.50	4.67	3.99	4.31	4.49	3.35	5.54

	Khristovite-(Ce) (Sokolova *et al.*, 1991)	Daissakisite-(Ce) (Rouse and Peacor, 1993)	Androsite-(La) (Bonazzi *et al.*, 1996)	*REE*-rich piemontite (Bonazzi *et al.*, 1996)	Ferriallanite-(Ce) (Kartashov *et al.*, 2003)	Allanite (Dollase, 1971)	Allanite (this study)
Si1	3.24	2.89	3.51	3.08	3.30	2.87	3.12
Si2	1.69	2.07	1.79	1.66	1.89	2.00	1.70
Si3	5.23	5.43	5.32	4.70	5.84	5.80	5.64

* Distortion for Si tetrahedra calculated according to the formula of $\sigma_{\theta(\mathrm{tet})}{}^2 = \sum_{i=1}^{6} (\theta_i - 109.47°)^a / 5.$

it shares an edge with the *A*2 polyhedron and the opposite edge with the *A*1 polyhedron. The *A*2 sites of epidote group minerals have the following occupancies: ($Ca_{1.00}$) and ($Ca_{0.98}Mn_{0.02}$) in epidote (Dollase, 1971; Gabe *et al*., 1973; Kvick *et al*., 1988), ($Ca_{0.84}Sr_{0.16}$) in piemontite (Ferraris *et al.*, 1989), ($Sr_{0.59}Ca_{0.41}$) and ($Sr_{0.73}Ca_{0.27}$) in strontiopiemontite (Bonazzi *et al*., 1990), ($Pb_{0.5}Sr_{0.25}(Ca,Mn)_{0.25}$) in hancockite (Dollase, 1971). On the other hand, the A*2* sites of allanites incorporate *REE*, Th and Mn. This incorporation indicates that there is a disordered distribution of these cations at *A*2 sites. Inasmuch as the distorted *A*2 polyhedron accommodating *REE* shares one O2−O2 edge with the Si3 tetrahedron (Fig. 6), it is reasonable that Si3 distortion of allanite is greater than that of the other epidote group minerals.

Figure 8 shows that distortions of averaged *A* and *M* sites of allanite from the Daibosatsu Pass can be distinguished from those of other epidote group minerals: they were calculated from average bond lengths following the modified method of Robinson *et al*. (1971). The dotted lines in Fig. 8 indicate that the *A*-site distortions of *REE*-bearing epidote group minerals (allanite zone) are larger than those of the other epidote group minerals (non-allanite zone). The larger distortion of *A* sites in allanites is caused by occupancy of *REE* at *A*2 sites. The bond valence sum was calculated to establish the credibility of the refined crystal structure. The calculation was carried out as by Brown and Altermatt (1985) with parameters given by Brese and O'Keeffe (1991). Bond valences of O2 and O8 are undersaturated in comparison with the ideal bond valence, 2.00, for an O atom (Table 5). The bond valence model does not necessarily give an unambiguous description for a defect environment (Brown, 2002). Moreover, undersaturation of bond valence sums for O2 and O8 are interpreted as the effect of defect at the *A*2 site. On the other hand, the bond valence sums for O4 and O10 are 1.73 and 1.22 v.u., respectively,

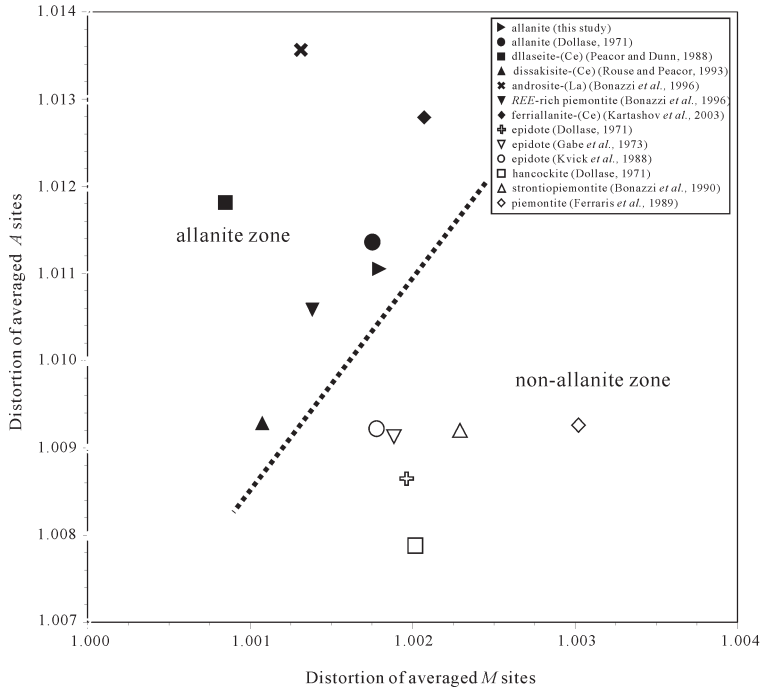

FIG. 8. Relationship between averaged distortions of *A* and *M* sites in epidote group minerals. The dotted line represents the boundary between allanites and the other epidote group minerals. The modified method of Robinson *et al.* (1971) is as follows:

(1) Equation for distortion of *A* sites: $\lambda_A = \frac{\lambda_{A1}+\lambda_{A2}}{2}$, where $\lambda_{A1} = \sum_{i=1}^{9}(l_i/l_0)^2/9$ for *A*1, $\lambda_{A2} = \sum_{i=1}^{10}(l_i/l_0)^2/10$ for the *A*2 site.

(2) Equation for distortion of *M* sites: $\lambda_M = \frac{\lambda_{M1}+\lambda_{M2}+\lambda_{M3}}{3}$, where $\lambda_M = \sum_{i=1}^{6}(l_i/l_0)^2/6$ for each *M* site.

implying that the O10 atom is the donor oxygen for the H atom (Table 5). A firm chemical bond exists between H and O10. The chemical bond between O10 and H in allanite is consistent with those in ferriallanite-(Ce) (Kartashov *et al*., 2002) and in epidote (Kvick *et al*., 1988). Table 12 topologically summarizes configurations of hydrogen bonds for epidote group minerals. The O4–O10 distance of the present allanite is observed to be 2.93 Å. For that reason, if O10–H and O4···H distances are presumed to be 0.96 and 1.97 Å, respectively, then the bond angle of O10–H···O4 will be 180º. The estimated O4–H distance, 1.97 Å, closely coincides with the 1.96 Å observed in epidote (Kvick *et al*., 1988). As shown in Table 12, the O10–H···O4 angle calculated for the present allanite is estimated to be practical for the allanite structure.

Allanite as an indicator of tectonic setting

The present interest in allanites from granitic rocks of the Japanese island arc originated from the fact that Th is present in all the samples despite the fact that no U was detected by EMPA. Therefore, this unique incorporation of Th has an implication for the crystallization mechanism of allanite in granitic rocks. However, some reports (e.g. Hasegawa, 1960; Suzuki *et al.*, 1990) concluded that allanites from granitic rocks in Japan often contain <0.1% U. It is rare for allanite to contain more U than Th (Gieré and Sorensen, 2004), e.g. in the metasomatically formed crystals from U-*REE* skarn (Maas *et al.*, 1987) and in the crystals occurring in blueschists from the Sanbagawa belt of Japan (Banno, 1993). These observations confirm that the allanites in granitic rocks from the Japanese island arc have experienced neither metasomatism nor metamorphism.

Incorporation of light *REE* and Th into allanites occurs in various rocks, having geochemical implications for their petrogenesis (Deer *et al*., 1986). The present (Tables 6, 7 and 8) and other studies (e.g. Hasegawa, 1960; Deer *et al*., 1986) suggest that allanites from the Japanese island arc are Th-bearing. Furthermore, they contain more Th than allanites from the other tectonic settings (Deer *et al*., 1986). Exley (1980) also reported values of up to 4.88 wt.% ThO_2 in allanites of the Skye granite of Tertiary continental margin

TABLE 12. Comparisons of interatomic distances and angles for hydrogen bonding in epidote group minerals.

	Epidote (Gabe *et al.*, 1973)	Epidote (Kvick *et al.*, 1988)	Piemontite (Ferraris *et al.*, 1989)	Strontiopiemontite (Bonazzi *et al.*, 1990)
O10–H	0.89	0.98	0.97	0.89
H···O4	2.02	1.96	2.00	2.17
O10–O4	2.90	2.92	2.96	2.98
O10–H···O4	173.7	166.9	168.1	149.9

	Dollaseite-(Ce) (Peacor and Dunn, 1988)	Khristovite-(Ce) (Sokolova *et al.*, 1991)	Daissakisite-(Ce) (Rouse and Peacor, 1993)	Androsite-(La) (Bonazzi *et al.*, 1996)
O10–H	0.96	0.91	0.77	0.88
H···O4	1.88	1.97	2.14	2.08
O10–O4	2.83	2.87	2.90	2.94
O10–H···O4	170.2	169.7	177.5	165.9

	REE-rich piemontite (Bonazzi *et al.*, 1996)	Ferriallanite-(Ce) (Kartashov *et al.*, 2002)	Allanite (this study)
O10–H	0.85	0.71	0.96 (constrained)
H···O4	2.10	2.18	1.97 (assumed)
O10–O4	2.94	2.89	2.93 (observed)
O10–H···O4	167.7	177.3	180.0 (calculated)

origin. The present observation that allanites from the Japanese island arc are rich in Th greatly reinforces the weight of Hermann's (2002) conclusion that allanite has the potential to be a major carrier of light *REE* and Th in subducted crustal materials.

This study compares the ternary Al_2O_3-Fe_2O_3-Σ*REE* compositions of allanites in granitic rocks from Japan with those of previously published data, clarifying the tectonic settings for allanite crystallization. Many allanites from granitic rocks were plotted in the ternary diagram in Fig. 9. Allanites from the island arc zone are plotted in Zone 2 between the continental margin zone (Zone 3) and the intracontinental one (Zone 1). This zoning depends on different Fe_2O_3 contents of allanites. In general, oxygen fugacities for intracontinental, island arc and continental margin zones set the following trend. Most Proterozoic anorogenic granites from Arizona and neighbouring California and Nevada (intracontinental) appear to have crystallized with oxygen fugacity (f_{O_2}) in the range $10^{-15.8}$–$10^{-14.5}$ bar at 700ºC (Anderson and Bender, 1989). On the other hand, the f_{O_2} of Cretaceous granitic complexes from Myoken-zan and Hobenzan, SW Japan is 10^{-17} bar at 700ºC (Takagi and Nureki, 1994; Nakashima, 1996). Therefore, the division into three zones in Fig. 9 is consistent with petrological data for the intracontinental and island arc areas. Nevertheless, there has been no report concerning the oxygen fugacity of granites from continental margin areas. Furthermore, an alternative interpretation of Fig. 9 might suggest that the oxygen fugacity of granites in the continental margin area is lower than that in the island arc area. The establishment of these three groups has implications for the different oxygen fugacities influencing the Fe_2O_3 content for allanite crystallization. Therefore, such a discrimination diagram is expected to be useful in trying to understand the origin of granitic magmas yielding allanites and trying to infer tectonic settings for their host rocks.

Conclusions

Based on crystal chemistry of the present allanites and structure refinement of the allanite under the constraint of its chemical composition, the following conclusions can be drawn:

(1) Allanites occurring in the present granitic rocks from the Japanese island arc were identified as allanite-(Ce).

(2) Global tectonic settings for allanite crystallization are implicit in their Fe_2O_3 content differences: three zones on the ternary Al_2O_3-Fe_2O_3-Σ*REE* diagram signify intracontinental, island arc, and continental margin zones in order of decreasing Fe_2O_3.

(3) Allanite is the important host for light *REE* and Th in trace element budgets of subduction zone processes.

(4) Two IR absorption bands at 3355 and 3187 cm^{-1} and the shift towards the lower wavenumber of the SiO-stretching band observed

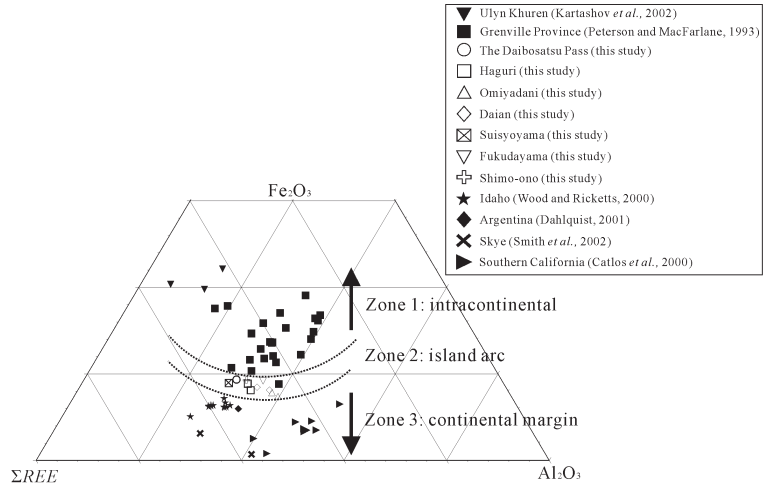

FIG. 9. Al_2O_3-Fe_2O_3-Σ*REE* diagram of allanites. The dashed lines indicate the three groups of different kinds of occurrence of allanite.

for the single allanite crystal serve as indicators of metamictization for allanite.

(5) Crystal chemical examination of allanites suggests that the isolated SiO_4 tetrahedron has the largest distortion, which is common to the epidote group minerals, and that the larger distortion of *A* sites in allanites can contrast well with smaller distortion of *A* sites in the other epidote group minerals because of occupancy of *REE* at *A*2 sites.

(6) The bond angles between the O10–H bond and hydrogen bond H···O4 range from 170º to 180º in the allanite groups.

Acknowledgements

Single crystal X-ray data collections and EMPA were carried out in the Chemical Analysis Centre, University of Tsukuba. We thank an anonymous reviewer for helpful comments and editorial assistant, Xiaojie Lou, for improving this manuscript.

References

Anderson, J.L. and Bender, E.E. (1989) Nature and origin of Proterozoic A-type granitic magmatism in the southwestern United States of America. *Lithos*, **23**, 19–52.

Banno, Y. (1993) Chromian sodic pyroxene, phengite and allanite from the Sanbagawa blueschists in the eastern Kii Peninsula, central Japan. *Mineralogical Journal*, **16**, 306–317.

Baur, W.H. (1981) Interatomic distance predictions for computer simulation of crystal structures. Pp. 31–52 in: *Structure and Bonding in Crystals II* (M. O'Keeffe and A. Navrotsky, editors). Academic Press, New York.

Bonazzi, P., Menchetti, S. and Palenzona, A. (1990) Strontiopiemontite, a new member of the epidote group, from Val Graveglia, Liguria, Italy. *European Journal of Mineralogy*, **2**, 519–523.

Bonazzi, P., Menchetti, S. and Reinecke, T. (1996) Solid solution between piemontite and androsite-(La), a new mineral of the epidote group from Andros Island, Greece. *American Mineralogist*, **81**, 735–742.

Brese, N.E. and O'Keeffe, M. (1991) Bond-valence parameters for solids. *Acta Crystallographica*, **B47**, 192–197.

Brown, I.D. (2002) Modelling inorganic structures. Pp. 161–162 in: *The Chemical Bond in Inorganic Chemistry*. Oxford University Press, New York.

Brown, I.D. and Altermatt, D. (1985) Bond-valence parameters obtained from a systematic analysis of the inorganic crystal structure database. *Acta Crystallographica*, **B41**, 244–247.

Burdett, J.K. (1995) Metals and insulators. Pp. 176–179 in: *Chemical Bonding in Solids*. Oxford University Press, New York.

Čech, F., Vrána, S. and Povondra, P. (1972) A non-metamict allanite from Zambia. *Neues Jahrbuch für Mineralogie Abhandlungen*, **116**, 208–223.

Chesner, C.A. and Ettlinger, A.D. (1989) Composition of volcanic allanite from the Toba Tuffs, Sumatra, Indonesia. *American Mineralogist*, **74**, 750–758.

Dana, J.D. (1911) Allanite. Pp. 522–526 in: *The System of Mineralogy of James Dwight Dana 1837–1868: Descriptive Mineralogy*. John Wiley & Sons, New York.

Deer, W.A., Howie, R.A. and Zussman, J. (1986) Allanite. Pp. 151–179 in: *Rock-forming Minerals*, 2nd ed., Vol. **1B**. Longman Scientific and Technical, Essex, England.

Dollase, W.A. (1971) Refinement of the crystal structures of epidote, allanite and hancockite. *American Mineralogist*, **56**, 447–464.

Ercit, T.S. (2002) The mess that is 'allanite'. *The Canadian Mineralogist*, **40**, 1411–1419.

Exley, R.A. (1980) Microprobe studies on REE-rich accessory minerals: implications for Skye granite petrogenesis and REE mobility in hydrothermal systems. *Earth and Planetary Science Letters*, **48**, 97–110.

Ferraris, G., Ivaldi, G., Fuess, H. and Gregson, D. (1989) Manganese/iron distribution in a strontian piemontite by neutron diffraction. *Zeitschrift für Kristallographie*, **187**, 145–151.

Gabe, E.J., Portheine, J.C. and Whitlow, S.H. (1973) A reinvestigation of the epidote structure: confirmation of the iron location. *American Mineralogist*, **58**, 218–223.

Gaines, R.V., Skinner, H.C.W., Foord, E.E., Mason, B. and Rosenzweig, A. (1997) Epidote Group. Pp. 1195–1205 in: *Dana's New Mineralogy.* John Wiley & Sons, New York.

Gieré, R. and Sorensen, S.S. (2004) Allanite and other REE-rich epidote-group minerals. Pp. 431–493 in: *Epidote* (A. Liebscher and G. Franz, editors). Reviews in Mineralogy and Geochemistry, **56**. Mineralogical Society of America and the Geochemical Society, Washington, D.C.

Goldschmidt, V. (1920) Orthit. Pp. 62–67 in: *Atlas der Krystallformen, Tafeln, Vol. 3*, Carl Winters Universitätsbuchhandlung, Heidelberg, Germany.

Hasegawa, S. (1957) Chemical studies of allanites and their associated minerals from the pegmatites in the northern part of the Abukuma Massif. *Science Report, University of Tohoku, Third series*, **5**, 345–371.

Hasegawa, S. (1960) Chemical composition of allanite. *Science Report, University of Tohoku, Third series*, **6**, 331–387.

Hayase, I. (1954) The radioactivity of rocks and minerals studied with nuclear emulsion. II. Thorium content of granitic allanites. *Memoirs of the College of Science, University of Kyoto*, **B21**, 171–182.

Hermann, J. (2002) Allanite: thorium and light rare earth element carrier in subducted crust. *Chemical Geology*, **192**, 289–306.

Hintze, C. (1897) Orthit. Pp. 257–276 in: *Handbuch der Mineralogie.* Verlag Von Veit & Comp, Leipzig, Germany.

Hutton, C.O. (1951) Allanite from Yosemite National Park, Tuolumne Co., California. *American Mineralogist*, **36**, 233–248.

Holtstam, D., Andersson, U.B. and Mansfeld, J. (2003) Ferriallanite-(Ce) from the Bastnäs deposit, Västmanland, Sweden. *The Canadian Mineralogist*, **41**, 1233–1240.

Janeczek, J. and Eby, R.K. (1993) Annealing of radiation damage in allanite and gadolinite. *Physics and Chemistry of Minerals*, **19**, 343–356.

Kartashov, P.M., Ferraris, G., Ivaldi, G., Sokolova, E. and McCammon, C.A. (2002) Ferriallanite-(Ce), $CaCeFe^{3+}AlFe^{2+}(SiO_4)(Si_2O_7)O(OH)$, a new member of the epidote group: description, X-ray and Mössbauer study. *The Canadian Mineralogist*, **40**, 1641–1648.

Kartashov, P.M., Ferraris, G., Ivaldi, G., Sokolova, E. and McCammon, C.A. (2003) Ferriallanite-(Ce), $CaCeFe^{3+}AlFe^{2+}(SiO_4)(Si_2O_7)O(OH)$, a new member of the epidote group: description, X-ray and Mössbauer study: errata. *The Canadian Mineralogist*, **41**, 829–830.

Ksenofontov, V.G., Laptienko, A.Ya., Ruban, I.V., Sukharevsky, B.Ya. and Pustovit, A.V. (1985) The influence of the crystalline field on the distortion of the octahedral complexes of divalent iron. *Solid State Communications*, **53**, 9–14.

Kvick, A., Pluth, J.J., Richardson Jr., J.W. and Smith, J.V. (1988) The ferric ion distribution and hydrogen bonding in epidote: a neutron diffraction study at 15 K. *Acta Crystallographica*, **B44**, 351–355.

Maas, R., McCulloch, M.T. and Campbell, I.H. (1987) Sm-Nd isotope systematics in uranium-rare earth element mineralization at the Mary Kathleen Uranium Mine, Queensland. *Economic Geology*, **82**, 1805–1826.

Mahood, G. and Hildreth, W. (1983) Large partition coefficients for trace elements in high-silica rhyolites. *Geochimica et Cosmochimica Acta*, **47**, 11–30.

Nagashima, O. and Nagashima, K. (1960) Allanite. Pp. 173–184 in: *The Rare Earth Minerals of Japan.* Chigakukenkyu-Kai, Kyoto, Japan (in Japanese).

Nakashima, K. (1996) Chemistry of Fe-Ti oxide minerals in the Hobenzan granitic complex, SW Japan: subsolidus reduction in relation to base metal mineralization. *Mineralogy and Petrology*, **58**, 51–69.

Nishida, N., Kimata, M. and Sugimoto, A. (1999) Quantitative electron-probe microanalysis of various kinds of rare-earth elements in minerals. *Journal of The Mineralogical Society of Japan*, **28**, 71–81 (in Japanese with English abstract).

North, A.C.T., Phillips, D.C. and Mathews, F.S. (1968) A semi-empirical method of absorption correction. *Acta Crystallographica*, **A24**, 351–359.

Oberli, F., Sommerauer, J. and Steiger, R.H. (1981) U-(Th)-Pb systematics and mineralogy of single crystals and concentrates of accessory minerals from the Cacciola granite, central Gotthard massif, Switzerland. *Schweizerische Mineralogische und Petrographische Mitteilungen*, **61**, 323–348.

Oberli, F., Meier, M., Berger, A., Rosenberg, C.L. and Gieré, R. (2004) U-Th-Pb and $^{230}Th/^{238}U$ disequilibrium isotope systematics: precise accessory mineral chronology and melt evolution tracing in the Alpine Bergell intrusion. *Geochimica et Cosmochimica Acta*, **68**, 2543–2560.

Peacor, D.R. and Dunn, P.J. (1988) Dollaseite-(Ce) (magnesium orthite redefined): structure refinement and implications for $F+M^{2+}$ substitutions in epidote-group minerals. *American Mineralogist*, **73**, 838–842.

Pellas, P. (1961) Métamictisation des allanites. Possibilité de déterminer des âges géologiques. *Académie des Sciences*, **252**, 3280–3282 (in French).

Peterson, R.C. and MacFarlane, D.B. (1993) The rare-earth-element chemistry of allanite from the Grenville Province. *The Canadian Mineralogist*, **31**, 159–166.

Pudovkina, Z.V. and Pyatenko, Yu.A. (1965) Crystal structure of nonmetamict orthite. *Doklady Akademii Nauk SSSR, Earth Sciences Sections*, **153**, 146–149.

Reed, S.J.B. and Buckley, A. (1998) Rare-earth element determination in minerals by electron-probe microanalysis: application of spectrum synthesis. *Mineralogical Magazine*, **62**, 1–8.

Robinson, K., Gibbs, G.V. and Ribbe, P.H. (1971) Quadratic elongation: a quantitative measure of distortion in coordination polyhedra. *Science*, **172**, 567–570.

Rouse, R.C. and Peacor, D.R. (1993) The crystal structure of dissakisite-(Ce), the Mg analogue of allanite-(Ce). *The Canadian Mineralogist*, **31**, 153–157.

Sakai, C., Higashino, T. and Enami, M. (1984) REE-bearing epidote from Sanbagawa pelitic schists, central Shikoku, Japan. *Geochemical Journal*, **18**, 45–53.

Sheldrick, G.M. (1997) *SHELXL-97. A program for the refinement of crystal structures.* University of

Göttingen, Germany.

Smith, M.P., Henderson, P. and Jeffries, T. (2002) The formation and alteration of allanite in skarn from the Beinn an Dubhaich granite aureole, Skye. *European Journal of Mineralogy*, **14**, 471–486.

Sokolova, E.V., Nadezhina, T.N. and Pautov, L.A. (1991) Crystal structure of a new natural silicate of manganese from the epidote group. *Soviet Physics: Crystallography*, **36**, 172–174.

Suzuki, K., Adachi, M. and Yamamoto, K. (1990) Possible effects of grain-boundary REE on the REE distribution in felsic melts derived by partial melting. *Geochemical Journal*, **24**, 57–74.

Takagi, T. and Nureki, T. (1994) Two T-f(O_2) paths in the Myoken-zan magnetite-bearing granitic complex, San'yo belt, southwestern Japan. *The Canadian Mineralogist*, **32**, 747–762.

Tröger, W.E. (1971) Optisch zweiachsige minerale: Nesosilikate, Sorosilikate. Pp. 56–59 in: *Optische Bestimmung der gesteinsbildenden Minerale, Teil 1 Bestimmungstabellen*. E. Schweizerbart'sche Verlagsbuchhandlung, Stuttgart, Germany.

Ueda, T. (1955) The crystal structure of allanite, $OH(Ca,Ce)_2(Fe^{3+},Fe^{2+})Al_2OSi_2O_7SiO_4$. *Memoirs of the College of Science*, *University of Kyoto*, **B22**, 145–163.

Ueda, T. (1957) Studies on the metamictization of radioactive minerals. *Memoirs of the College of Science*, *University of Kyoto*, **B24**, 81–120.

Uchiyama, I., Watanabe, Y. and Kimoto, S. (1972) Quantitative analysis. Pp. 114–115 in: *X-ray Micro Analyzer*. The Nikkan Kougyou Shinbun, Tokyo (in Japanese).

Wickleder, M.S. (2002) Inorganic lanthanide compounds with complex anions. *Chemical Reviews*, **102**, 2011–2087.

Wing, B.A. Ferry, J.M. and Harrison, T.M. (2003) Prograde destruction and formation of monazite and allanite during contact and regional metamorphism of pelites: petrology and geochronology. *Contributions to Mineralogy and Petrology*, **145**, 228–250.

Wood, S.A. and Ricketts, A. (2000) Allanite-(Ce) from the Eocene Casto granite, Idaho: response to hydrothermal alteration. *The Canadian Mineralogist*, **38**, 81–100.

Yang, J.J. and Enami, M. (2003) Chromian dissakisite-(Ce) in a garnet lherzolite from the Chinese Su-Lu UHP metamorphic terrane: implication for Cr incorporation in epidote-group minerals and recycling of REE into the Earth's mantle. *American Mineralogist*, **88**, 604–610.

Zhang, M. and Salje, E.K.H. (2001) Infrared spectroscopic analysis of zircon: Radiation damage and the metamict state. *Journal of Physics: Condensed Matter*, **13**, 3057–3071.

[*Manuscript received 24 July 2004: revised 22 June 2005*]